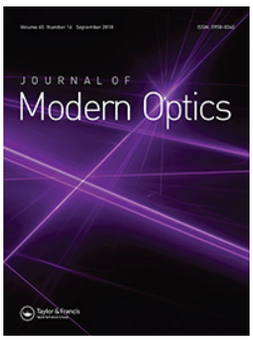

Journal of Modern Optics

ISSN: 0950-0340 (Print) 1362-3044 (Online) Journal homepage: https://www.tandfonline.com/loi/tmop20

Alignment algorithm for three-mirror anastigmatic telescopes based on nodal aberration theory

Zhenchong Xing, Yongfeng Hong, Xiaobin Zhang & Bao Zhang

To cite this article: Zhenchong Xing, Yongfeng Hong, Xiaobin Zhang & Bao Zhang (2018) Alignment algorithm for three-mirror anastigmatic telescopes based on nodal aberration theory, Journal of Modern Optics, 65:16, 1910-1919, DOI: 10.1080/09500340.2018.1471531

To link to this article: https://doi.org/10.1080/09500340.2018.1471531

Published online: 11 May 2018.

JOURNAL OF MODERN OPTICS
2018, VOL. 65, NO. 16, 1910–1919
https://doi.org/10.1080/09500340.2018.1471531

Taylor & Francis
Taylor & Francis Group

Alignment algorithm for three-mirror anastigmatic telescopes based on nodal aberration theory

Zhenchong Xing[a,b], Yongfeng Hong[a], Xiaobin Zhang[a] and Bao Zhang[a]

[a]Changchun Institute of Optics, Fine Mechanics and Physics, Chinese Academy of Science, Changchun, People's Republic of China; [b]University of Chinese Academy of Science, Beijing, People's Republic of China

ABSTRACT

For most of the alignment algorithms, alignment errors and figure errors cannot be separated due to the coupling effect among optical elements. We present an alignment algorithm for TMA telescopes on the framework of nodal aberration theory (NAT). Based on NAT, we firstly determine the axial misalignments of secondary (SM) and tertiary (TM) mirrors. Then we decouple the lateral misalignments and angular misalignments of SM and TM. Finally, we decouple the figure errors of primary mirror (PM) from the alignment errors of SM and TM. To validate the algorithm, a TMA telescope is designed for simulation. In the simulation, modulation transfer function (MTF) is chosen to evaluate the telescope before and after correction. It is found that the algorithm presented in this paper maintains high precision. In the end, a Monte Carlo simulation is conducted to further demonstrate the accuracy of the presented alignment algorithm even in poor conditions.

ARTICLE HISTORY
Received 27 December 2017
Accepted 25 April 2018

KEYWORDS
Aberration theory; alignments; telescopes; active optics

1. Introduction

To improve resolution and performance, large-aperture astronomical telescopes with fast F number need to be constructed. But such telescopes are easily perturbed because of the effect of thermal variation, gravity, vibration and other factors. Then telescope systems become different from the designed. Optical elements may become misaligned and mirror figures may also be deformed, all of which will result severe degradation of the image quality. To maintain perfect performance, active optics system needs to be integrated in the telescope.

The concept of active optics system has been presented for nearly four decades. It was first applied to New Technology Telescope (NTT) (*1*). Since then, many telescopes (either monolithic or segmented) integrated with active optics system have been constructed or under construction. The main task of active optics system is to recover the perturbed telescope system. To achieve that, all the perturbations (including alignment errors and figure errors) should be solved firstly.

There are several algorithms that can be used to solve these perturbations in active optics system, for instance, sensitivity table method (STM), merit function regression (MFS) method, differential wave-front sampling (DWS) method, nodal aberration theory (NAT) method, etc. All the algorithms are based on the idea of system optimization. In general, the perturbed system can be recovered based on any algorithm, if the system owns fewer perturbation parameters. But for multi components optical system, the perturbed system may be optimized to a local optimum, where the system owns perfect performance, but it is different from the original system. The reason is that there exists coupling effect among optical elements.

For multi components optical system, both STM (*2*, *3*) and MFS method (*4*) cannot separate the coupling effect. The reason is that they are based on the least square method (LSM), which is numerical. The perturbations resulting from them are not correct to some extent. To eliminate the coupling effect, an algorithm called DWS was presented (*5*, *6*). This method can analytically separate the coupling effect. While considering its high sensitivity to the environment, such algorithm is difficult to achieve in the practical application. Besides, another algorithm, which is based on NAT, can also decouple the optical elements. This algorithm can analytically relate perturbations with wave aberration coefficients. And it is

CONTACT Zhenchong Xing chong091010123@163.com Changchun Institute of Optics, Fine Mechanics and Physics, Chinese Academy of Science, Changchun 130033, People's Republic of China

not limited to the environment. So this algorithm is of great advantage. More attention should be paid to it.

Recently, the method based on NAT has been studied in different kinds of telescopes. Manuel (*7*) studied the functional aberration description of a misaligned R–C telescope. Schmid et al. (*8*) separated the effects of astigmatic figure error from misalignments. Sebag et al. (*9*) presented an alignment plan including the primary mirror (PM) figure errors for the Large Synoptic Survey Telescope (LSST). Gu et al. (*10*) simulated the alignment of a three-mirror anastigmatic (TMA) telescope. Schmid et al. (*11*) presented an alignment method of the two-mirror telescope.

In (*10*), an alignment algorithm for the TMA telescope based on NAT has been studied. But there are two great shortages in the alignment algorithm. On one hand, there are two larger residual misalignments (YDE_{PM}, YDE_{SM}) remained, which means the telescope is not recovered and it is still misaligned. On the other hand, only lateral misalignments (*XDE*, *YDE*) and angular misalignments (*ADE*, *BDE*) are considered in (*10*). Axial misalignments (*ZDE*) and figure errors ($C_5/C_6, C_{10}/C_{11}$), which are also easily introduced, are not included in the alignment algorithm. To cover these shortages, a more comprehensive alignment algorithm should be modelled. To model this algorithm, some new work has to be done in this paper.

2. NAT for the TMA telescope

The vector form of wave aberration expansion for rotationally symmetric optical system is the theoretical basis of NAT. It was converted from the scalar form presented by Hopkins (*12*) and disseminated by Shack (*13*) and Thompson and Rolland (*14*). The vector form is expressed as:

$$W = \sum_j \sum_p^{\infty} \sum_n^{\infty} \sum_m^{\infty} (W_{klm})_j (\vec{H}\cdot\vec{H})^p (\vec{\rho}\cdot\vec{\rho})^n (\vec{H}\cdot\vec{\rho})^m, \quad k = 2p+m, l = 2n+m, \tag{1}$$

where $\vec{H}$ denotes the normalized field vector, $\vec{\rho}$ denotes the normalized radial vector as described in (*15*). When the rotational symmetry is broken in an optical system, a sigma vector ($\vec{\sigma}_j$) representing the displacement of the centre of the aberration field was introduced by Buchroeder (*16*). And the effective field height ($\vec{H}-\vec{\sigma}_j$) will replace the normalized field vector $\vec{H}$ in Equation (1) to describe the characteristic aberration fields after perturbation. Note that the total wave aberration in image plane is the sum of individual surface contributions in either rotationally or non-rotationally symmetric optical system.

As described in NAT, sigma vector must be separated into two components in the case of an aspheric surface. One indicates the contribution associated with spherical base curve, the other indicates the contribution associated with aspheric departure from the spherical base curve. They will be distinguished by using superscript *sph* and *asph* respectively. In TMA telescopes, PM, secondary mirror (SM) and tertiary mirror (TM) are all aspheric. And PM is usually regarded as the reference. SM and TM are perturbed with respect to PM. Hence the sigma vectors of SM and TM should be divided into two parts. Note that the reference of the TMA telescope in (*10*) is TM. So some equations will be modified to accurately represent the telescope in this paper. According to the paraxial ray-tracing depicted in Figure 1 and the optical axis ray-tracing depicted in Figure 2, the quantitative relationships between sigma vectors and perturbations can be determined based on Eq. (3) and Eq. (10) in (*10*). For simplicity, the specific relationships can be described as:

$$\sigma_{SM,y}^{asph} = -\frac{YDE_{SM}}{d_1 \bar{u}_{PM}},$$

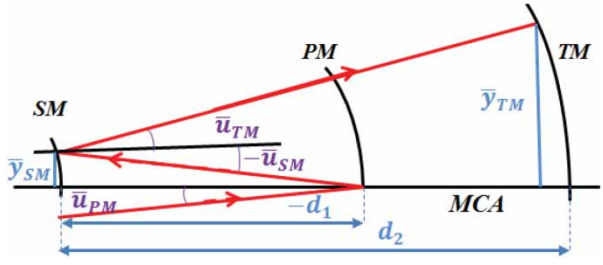

Figure 1. Layout of paraxial ray-tracing for TMA telescope. Red line represents paraxial chief ray. MCA is the abbreviation of mechanical coordinate axis, which is coincident with the optical axis of PM if PM is referred.

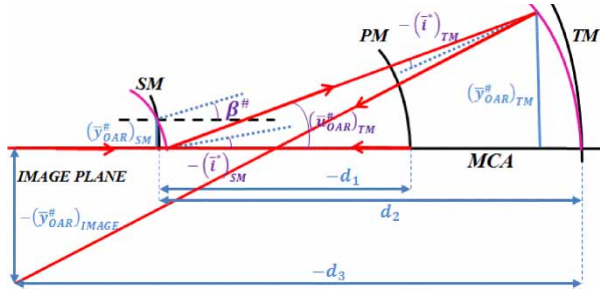

Figure 2. Layout of optical axis ray-tracing for TMA telescope. Red line represents optical axis ray. Pink lines represent the state of SM and TM after perturbation. Note that all the quantities referring to MCA or the axis parallel to MCA are denoted with a pound sign. And all the quantities referring to optical axis ray (OAR) are denoted with an asterisk.

$$\sigma_{SM,y}^{sph} = -\frac{ADE_{SM} + c_{SM}YDE_{SM}}{(1 + c_{SM}d_1)\bar{u}_{PM}},$$
$$\sigma_{TM,y}^{asph} = \frac{YDE_{TM} - 2d_2(ADE_{SM} + c_{SM}YDE_{SM})}{[d_2 + d_1(2c_{SM}d_2 - 1)]\bar{u}_{PM}},$$
$$\sigma_{TM,y}^{sph} = \frac{\begin{array}{c}ADE_{TM} + c_{TM}YDE_{TM}\\ -2(1 + c_{TM}d_2)(ADE_{SM} + c_{SM}YDE_{SM})\end{array}}{[c_{TM}(d_2 - d_1) + 2c_{SM}(c_{TM}d_1d_2 + d_1) + 1]\bar{u}_{PM}}, \quad (2)$$

where all the symbols are defined as the same in the appendix in (*10*). Here only y-components of sigma vectors are discussed. Their x-components are ignored because of their similarity. And all the functions in Equation (2) are linear. All the perturbations can be solved in sequence if the sigma vectors are determined. The determination of the sigma vectors will be discussed in the following sections.

3. Boresight error for the TMA telescope

As shown in Figure 3, the intersection height of OAR with respect to Mechanical axis coordinate (MAC) is nonzero while the telescope is perturbed. This nonzero parameter is called boresight error. It can be deduced from Figure 2. Similar to sigma vectors, only y-component of the boresight error is discussed here. According to the derivation, we can see that boresight error is only dependent on the sigma vector associated with spherical component. The specific relationship can be given by

$$\begin{aligned} H_{TM,y}^{OAR} &= -2d_2[\bar{u}_{PM}(1 + d_1c_{SM})]\sigma_{SM,y}^{sph},\\ H_{IMAGE,y}^{OAR} &= -2(d_2 + d_3)[\bar{u}_{PM}(1 + d_1c_{SM})]\sigma_{SM,y}^{sph}\\ &\quad + 2d_3[c_{TM}(d_2 - d_1) + 2c_{SM}(c_{TM}d_1d_2 + d_1)\\ &\quad + 1]\bar{u}_{PM}\sigma_{TM,y}^{sph}, \end{aligned} \quad (3)$$

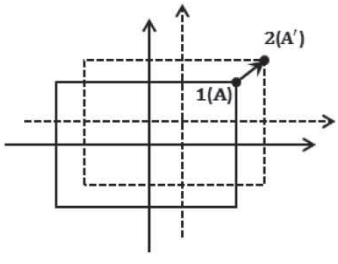

Figure 3. Schematic representation for the boresight error. Solid line represents the image plane of the nominal design. Dashed line represents the image plane after misalignment. The boresight error can be regarded as the vector, which is from point 1 to point 2.

where d_1, d_2, d_3 are the thickness of PM, SM, TM in nominal design, c_{SM}, c_{SM} are the curvatures of SM and TM. $H_{TM,y}^{OAR}$ denotes the intersection height of OAR with TM, $H_{IMAGE,y}^{OAR}$ denotes the intersection height of OAR with image plane. They are both linear with sigma vectors. So, sigma vectors contributed from spherical component can be determined if these two values can be accurately measured. However, the quantity $H_{TM,y}^{OAR}$ cannot be directly measured. Some means must be taken to determine it. In practical application, this parameter can be measured by inserting a beam splitter mirror between SM and TM. But this method weakens optical energy on the astronomical image plane. It is unwise and inadvisable.

Equation (3) denotes that the sigma vector with respect to SM is firstly determined. Then the sigma vector with respect to TM is determined. So, the measurement of $H_{TM,y}^{OAR}$ is in need. But there is no need to measure $H_{TM,y}^{OAR}$ if the processing sequence of sigma vectors is reversed. There is a field stop between SM and TM in TMA telescope. Only TM has some influence to the image of the field stop. So, the sigma vector contributed from TM can be determined based on the displacement of the image of the field stop. Then another sigma vector contributed from SM can be determined by using the fathomable boresight error on the image plane of the telescope. The specific expression is given by

$$\begin{aligned} H_{TM,y}^{FS} &= 2d_3[c_{TM}(d_2 - d_1) + 2c_{SM}(c_{TM}d_1d_2 + d_1)\\ &\quad + 1]\bar{u}_{PM}\sigma_{TM,y}^{sph},\\ H_{IMAGE,y}^{OAR} &= -2(d_2 + d_3)[\bar{u}_{PM}(1 + d_1c_{SM})]\sigma_{SM,y}^{sph}\\ &\quad + 2d_3[c_{TM}(d_2 - d_1) + 2c_{SM}(c_{TM}d_1d_2 + d_1)\\ &\quad + 1]\bar{u}_{PM}\sigma_{TM,y}^{sph}, \end{aligned} \quad (4)$$

where $H_{TM,y}^{FS}$ denotes the displacement of the image of the field stop. Based on Equation (4), the sigma vectors contributed from spherical component can be determined. However, the thicknesses in Equation (4) are unknown if there exist axial misalignments in TMA telescopes. So, the axial misalignments must be firstly determined.

Here we adopt the idea of Phase Diversity (PD) that wave-front aberrations can be obtained by analysing the focal image and defocus image. If the defocus distance of image plane is known, we can use Equation (4) before and after defocusing to determine the axial misalignments. Equation (4) before defocusing can be expressed by:

$$H_{TM,y,before}^{FS} = 2d_3'(c_{TM}YDE_{TM} + ADE_{TM}),$$

$$H^{OAR}_{SM+TM,y,before} = 2(d'_2 - d'_3 - 2c_{TM}d'_2d'_3)(c_{SM}YDE_{SM} + ADE_{SM}) + 2d'_3(c_{TM}YDE_{TM} + ADE_{TM}). \quad (5)$$

Equation (4) after defocusing can be expressed by:

$$H^{FS}_{TM,y,after} = 2(d'_3 - \Delta)(c_{TM}YDE_{TM} + ADE_{TM}),$$
$$H^{OAR}_{SM+TM,y,after} = 2[d'_2 - (d'_3 - \Delta) - 2c_{TM}d'_2(d'_3 - \Delta)](c_{SM}YDE_{SM} + ADE_{SM}) + 2(d'_3 - \Delta)(c_{TM}YDE_{TM} + ADE_{TM}), \quad (6)$$

where d'_2 and d'_3 denote the thicknesses of SM and TM after axial misalignment, they are given by$d'_2 = d_2 + ZDE_{TM} - ZDE_{SM}$, $d'_3 = d_3 - ZDE_{TM}$, Δ denotes the amount of defocus. Based on Equation (5) and Equation (6), the axial misalignments of SM and TM (ZDE_{TM} and ZDE_{SM}) can be determined as followed. Thus the sigma vectors associated with spherical component can be determined based on Equation (4).

$$ZDE_{TM} = d_3 - d'_3 = d_3 - \frac{\Delta}{1 - (H^{FS}_{TM,y,after}/H^{FS}_{TM,y,before})}, \quad (7)$$

$$ZDE_{SM} = d_2 + ZDE_{TM} - d'_2, = d_2 + ZDE_{TM} - \frac{\Delta + d'_3\left(\frac{(H^{OAR}_{SM+TM,y,after}) - (H^{FS}_{TM,y,after})}{(H^{OAR}_{SM+TM,y,before}) - (H^{FS}_{TM,y,before})} - 1\right)}{\left(\frac{(H^{OAR}_{SM+TM,y,after}) - (H^{FS}_{TM,y,after})}{(H^{OAR}_{SM+TM,y,before}) - (H^{FS}_{TM,y,before})} - 1\right)} \cdot -2c_{TM}\left[\Delta + d'_3\left(\frac{(H^{OAR}_{SM+TM,y,after}) - (H^{FS}_{TM,y,after})}{(H^{OAR}_{SM+TM,y,before}) - (H^{FS}_{TM,y,before})} - 1\right)\right] \quad (8)$$

Therefore, boresight error plays an important role not only in determining axial misalignments, but also in determining the sigma vectors associated with spherical component. More importantly, it is not negligible in practical application. Just as described in Advanced Technology Solar Telescope (ATST) (*17*, *18*), image boresight should be maintained during operation. If the image boresight is not maintained, the data obtained from wave-front sensing is inaccurate for the alignment algorithm. As shown in Figure 3, assuming that there is a detector (used for wave-front sensing) in position 1, it corresponds to a field point A. The field point A will move to position 2 if boresight error is introduced in the system. Then position 1 will correspond to an unknown field point. Obviously, the aberration coefficients obtained from position 1 and position 2 are different. But they are thought to be the same in the algorithm. So, the model is not correct at this moment. Therefore, the boresight error must be considered in order to establish the correct model.

4. Field dependences of third-order and fifth-order aberrations

Besides the expression in Equation (1), wave-front aberration can also be described as a sum of weighted Zernike polynomial. The polynomial can be expressed as:

$$W = \sum_j C_j Z_j(\rho, \varphi), \quad (9)$$

where $Z_j(\rho, \varphi)$ represents the j-th Zernike polynomial and its aperture dependence, C_j represents the scale of the corresponding Zernike polynomial and its field dependence.

Recently, Gray and Rolland (*19*) have expressed the wave-front aberration in terms of Zernike polynomial. In (*19*), Eq. (39) describes the aberration fields of the perturbed system. On the basis, we can get the field dependences of the corresponding Zernike polynomial.

As concluded by Gu and collaborators (*10*), the accuracy of the alignment model is lower only using third-order aberration theory. To obtain the accurate results, third-order and fifth-order aberration theory should be considered simultaneously. In this paper, we will not only focus on the alignment errors of the TMA telescopes, but also the figure errors. This means the number of the parameters needed to be determined has increased. Therefore, fifth-order or higher order aberration theory must be considered.

In perturbed optical systems, the vector forms of third-order and fifth-order aberrations have been deduced and analysed in (*20*–*22*). Combining them with Eq. (39) in (*19*), the field dependences of third-order and fifth-order aberrations can be exactly determined. In the following, the field dependences of third-order and fifth-order aberrations will be expanded into matrix form.

4.1. Fifth-order field-linear coma and oblique spherical aberration

As described by Thompson, the vector form of fifth-order field-linear coma is expressed following:

$$W = [(W_{151}\vec{H} - \vec{A}_{151}) \cdot \vec{\rho}](\vec{\rho} \cdot \vec{\rho})^2. \quad (10)$$

Its expansion based on vector multiplication can be written as:

$$W = \begin{bmatrix} W_{151}H_x - \vec{A}_{151,x} \\ W_{151}H_y - \vec{A}_{151,y} \end{bmatrix}^T \begin{bmatrix} |\vec{\rho}|^5 \cos\varphi \\ |\vec{\rho}|^5 \sin\varphi \end{bmatrix}. \quad (11)$$

To find the exact correspondence between Equation (10) and Equation (11), the aperture dependence of Equation (11) should be further expanded, followed by:

$$\begin{aligned} &\begin{bmatrix} |\vec{\rho}|^5 \cos\varphi \\ |\vec{\rho}|^5 \sin\varphi \end{bmatrix} \begin{bmatrix} |\vec{\rho}|^5 \cos\varphi \\ |\vec{\rho}|^5 \sin\varphi \end{bmatrix} \\ &= \frac{1}{10}\begin{bmatrix} (10|\vec{\rho}|^5 - 12|\vec{\rho}|^3 + 3|\vec{\rho}|)\cos\varphi \\ (10|\vec{\rho}|^5 - 12|\vec{\rho}|^3 + 3|\vec{\rho}|)\sin\varphi \end{bmatrix} \\ &\quad + \frac{4}{10}\begin{bmatrix} (3|\vec{\rho}|^3 - 2|\vec{\rho}|)\cos\varphi \\ (3|\vec{\rho}|^3 - 2|\vec{\rho}|)\sin\varphi \end{bmatrix} + \Delta, \end{aligned} \quad (12)$$

where $\begin{bmatrix} (10|\vec{\rho}|^5 - 12|\vec{\rho}|^3 + 3|\vec{\rho}|)\cos\varphi \\ (10|\vec{\rho}|^5 - 12|\vec{\rho}|^3 + 3|\vec{\rho}|)\sin\varphi \end{bmatrix} = \begin{bmatrix} Z_{14} \\ Z_{15} \end{bmatrix}$, $\begin{bmatrix} (3|\vec{\rho}|^3 - 2|\vec{\rho}|)\cos\varphi \\ (3|\vec{\rho}|^3 - 2|\vec{\rho}|)\sin\varphi \end{bmatrix} = \begin{bmatrix} Z_7 \\ Z_8 \end{bmatrix}$, Δ denotes x-tilt and y-tilt of the wave-front aberration. Therefore, a conclusion is done that fifth-order field-linear coma have certain contributions to C_7/C_8 if C_{14}/C_{15} is not small enough to be ignored. And the field dependences of the corresponding Zernike coefficients are determined, described by:

$$\begin{bmatrix} W_{151}H_x - \vec{A}_{151,x} \\ W_{151}H_y - \vec{A}_{151,y} \end{bmatrix} = 10\begin{bmatrix} C_{14} \\ C_{15} \end{bmatrix}. \quad (13)$$

Thompson also described the vector form of oblique spherical aberration, followed by:

$$W = \frac{1}{2}[(W_{242}\vec{H}^2 - 2\vec{H}\vec{A}_{242} + \vec{B}^2_{242}) \cdot \vec{\rho}^2](\vec{\rho} \cdot \vec{\rho}). \quad (14)$$

As done to fifth-order field-linear coma, Equation (14) should be expanded based on its aperture dependence. Through expansion and combination, a similar conclusion can be acquired that the values of Zernike coefficients C_5/C_6 have some contributions from oblique spherical aberration. And the field dependences of the corresponding Zernike coefficients are also determined, described by:

$$\begin{aligned} &\begin{bmatrix} H_x^2 - H_y^2 & -2H_x & 2H_y & 1 & 0 \\ 2H_xH_y & -2H_y & -2H_x & 0 & 1 \end{bmatrix} \begin{bmatrix} W_{242} \\ \vec{A}_{242,x} \\ \vec{A}_{242,y} \\ \vec{B}^2_{242,x} \\ \vec{B}^2_{242,y} \end{bmatrix} \\ &= 8\begin{bmatrix} C_{12} \\ C_{13} \end{bmatrix}. \end{aligned} \quad (15)$$

4.2. Third-order coma and field-cubed coma

To our knowledge, the aperture dependence of third-order coma is third. When fifth-order aberration is considered, field-cubed coma should be combined to third-order coma because of the same aperture dependence. The combining wave aberration expansion is followed

$$W = \begin{bmatrix} W_{331M}(\vec{H} \cdot \vec{H})\vec{H} - 2(\vec{H} \cdot \vec{A}_{331M})\vec{H} \\ +(W_{131} + 2B_{331M})\vec{H} \\ -(\vec{H} \cdot \vec{H})()\vec{A}_{331M} + \vec{B}^2_{331M}\vec{H}^* \\ -(\vec{A}_{131} + \vec{C}_{331M}) \end{bmatrix} \cdot \vec{\rho}(\vec{\rho} \cdot \vec{\rho}). \quad (16)$$

According to the aperture dependence in Equation (16), Z_7/Z_8 are its corresponding Zernike polynomials and C_7/C_8 are its corresponding Zernike coefficients. Recalling to Section 4.1, fifth-order field-linear coma also have some contributions to seventh and eighth Zernike coefficients. Through expansion and merging, the same matrix referred to Zhiyuan Gu can be obtained (*10*). A simplification is done here to reduce the needed fields of view in the calculation.

Note that sigma vector is much less than 1 in non-rotationally symmetric TMA systems. So the value of $\vec{B}^2_{311M}$ and B_{311M}, which are proportional to the squared value of sigma vector, are small enough to neglect compared to the low-order terms of sigma vector. And the value of $\vec{C}_{311M}$ is smaller. By omitting the higher order terms related to sigma vectors, Equation (16) can be simplified by:

$$\begin{aligned} &\begin{bmatrix} H_x^3 + H_xH_y^2 & H_x^2H_y + H_y^3 \\ -3H_x^2 - H_y^2 & -2H_xH_y \\ -2H_xH_y & -H_x^2 - 3H_y^2 \\ H_x & H_y \\ -1 & 0 \\ 0 & -1 \end{bmatrix}^T \begin{bmatrix} W_{331M} \\ \vec{A}_{331M,x} \\ \vec{A}_{331M,y} \\ W_{131} \\ \vec{A}_{131,x} \\ \vec{A}_{131,y} \end{bmatrix} \\ &= 3\begin{bmatrix} C_7 - 4C_{14} \\ C_8 - 4C_{15} \end{bmatrix}. \end{aligned} \quad (17)$$

4.3. Third-order astigmatism and fifth-order astigmatism

Similar to third-order coma and field-cubed coma, third-order astigmatism and fifth-order astigmatism also have the same aperture dependence. That means they have individual contributions to the same Zernike coefficients. Consequently, they should be merged together as

expressed:

$$W=\begin{bmatrix} \frac{1}{2}W_{422}(\vec{H}\cdot\vec{H})\vec{H}^2-(\vec{H}\cdot\vec{H})(\vec{H}\vec{A}_{422}) \\ +\frac{3}{2}(\vec{H}\cdot\vec{H})\vec{B}^2_{422}-(\vec{H}\cdot\vec{A}_{422})\vec{H}^2 \\ +\frac{1}{2}(W_{222}+3B_{422})\vec{H}^2-\frac{1}{2}\vec{H}(\vec{A}_{222}+3\vec{C}_{422}) \\ -\frac{1}{2}\vec{C}^3_{422}\vec{H}^*+\frac{1}{2}(\vec{D}^2_{422}+\vec{B}^2_{222}) \end{bmatrix}\cdot\vec{\rho}^2. \tag{18}$$

Oblique spherical aberration should also be considered when Equation (18) is expanded. After the higher order terms with respect to sigma vectors are omitted, the final result can be expressed as a matrix, given by:

$$\begin{bmatrix} H_x^4-H_y^4 & 2H_xH_y(H_x^2+H_y^2) \\ -4H_x^3 & -6H_x^2H_y-2H_y^3 \\ 4H_y^3 & -2H_x^2-6H_xH_y^2 \\ H_x^2-H_y^2 & 2H_xH_y \\ -H_x & -H_y \\ H_y & -H_x \\ 1 & 0 \\ 0 & 1 \end{bmatrix}^T \begin{bmatrix} W_{422} \\ \vec{A}_{422,x} \\ \vec{A}_{422,y} \\ W_{222} \\ 2\vec{A}_{222,x} \\ 2\vec{A}_{222,y} \\ \vec{B}^2_{222,x} \\ \vec{B}^2_{222,y} \end{bmatrix} = 2\begin{bmatrix} C_5-3C_{12} \\ C_6-3C_{13} \end{bmatrix}. \tag{19}$$

4.4. Elliptical coma

Elliptical coma (also called trefoil) is a typical wave aberration similar to third-order astigmatism. This kind of aberration almost remains unchanged when alignment errors are introduced. Its value mainly depends on the changes of the surface figures produced by three-point support. The vector form of elliptical coma has also been summarized, which follows:

$$W=\frac{1}{4}(W_{333}\vec{H}^3-3\vec{H}^2\vec{A}_{333}+3\vec{H}\vec{B}^2_{333}-\vec{C}^3_{333})\cdot\vec{\rho}^3. \tag{20}$$

Not like other wave-front aberrations, trefoil has contribution to Zernike coefficients C_{10}/C_{11}. Through simplification, a matrix could be derived, which is expressed by:

$$\begin{bmatrix} H_x^3-3H_xH_y^2 & 3H_x^2H_y-H_y^3 \\ -3H_x^2+3H_y^2 & -6H_xH_y \\ 6H_xH_y & -3H_x^2+3H_y^2 \\ 3H_x & 3H_y \\ -3H_y & 3H_x \\ -1 & 0 \\ 0 & -1 \end{bmatrix}^T \begin{bmatrix} W_{333} \\ \vec{A}_{333,x} \\ \vec{A}_{333,y} \\ \vec{B}^2_{333,x} \\ \vec{B}^2_{333,y} \\ \vec{C}^3_{333,x} \\ \vec{C}^3_{333,y} \end{bmatrix} = 4\begin{bmatrix} C_{10} \\ C_{11} \end{bmatrix}. \tag{21}$$

As discussed above, every single Zernike coefficient has specific field dependence. According to the field dependences, all the parameters associated with sigma vectors (perturbation vectors and scalars in the appendix) can be determined. Here we will focus more on one kind of perturbation vector, which is linear to the sigma vectors, given by:

$$\vec{A}_{klm}=W^{sph}_{klm,SM}\vec{\sigma}^{sph}_{SM}+W^{asph}_{klm,SM}\vec{\sigma}^{asph}_{SM}+W^{sph}_{klm,TM}\vec{\sigma}^{sph}_{TM}+W^{asph}_{klm,TM}\vec{\sigma}^{asph}_{TM}, \tag{22}$$

where W_{klm} denotes the Seidel coefficient of every optical component. Their values are confirmed with respect to the designed system. In order to determine the values of these sigma vectors, two more analogous equations are needed including Equation (4). The process of determining the values of these sigma vectors are followed: (here boresight errors and astigmatic field and comatic field are chosen)

$$\begin{aligned} H^{FS}_{TM,x}&=2d_3[c_{TM}(d_2-d_1)+2c_{SM}(c_{TM}d_1d_2+d_1)+1]\bar{u}_{PM}\sigma^{sph}_{TM,x}, \\ H^{FS}_{TM,y}&=2d_3[c_{TM}(d_2-d_1)+2c_{SM}(c_{TM}d_1d_2+d_1)+1]\bar{u}_{PM}\sigma^{sph}_{TM,y}, \\ H^{OAR}_{IMAGE,x}&=-2(d_2+d_3)[\bar{u}_{PM}(1+d_1c_{SM})]\sigma^{sph}_{SM,x}+2d_3[c_{TM}(d_2-d_1)+2c_{SM}(c_{TM}d_1d_2+d_1)+1]\bar{u}_{PM}\sigma^{sph}_{TM,x}, \\ H^{OAR}_{IMAGE,y}&=-2(d_2+d_3)[\bar{u}_{PM}(1+d_1c_{SM})]\sigma^{sph}_{SM,y}+2d_3[c_{TM}(d_2-d_1)+2c_{SM}(c_{TM}d_1d_2+d_1)+1]\bar{u}_{PM}\sigma^{sph}_{TM,y}, \\ \vec{A}_{222,x}&=W^{sph}_{222,SM}\vec{\sigma}^{sph}_{SM,x}+W^{asph}_{222,SM}\vec{\sigma}^{asph}_{SM,x}+W^{sph}_{222,TM}\vec{\sigma}^{sph}_{TM,x}+W^{asph}_{222,TM}\vec{\sigma}^{asph}_{TM,x}, \\ \vec{A}_{222,y}&=W^{sph}_{222,SM}\vec{\sigma}^{sph}_{SM,y}+W^{asph}_{222,SM}\vec{\sigma}^{asph}_{SM,y}+W^{sph}_{222,TM}\vec{\sigma}^{sph}_{TM,y}+W^{asph}_{222,TM}\vec{\sigma}^{asph}_{TM,y}, \\ \vec{A}_{131,x}&=W^{sph}_{131,SM}\vec{\sigma}^{sph}_{SM,x}+W^{asph}_{131,SM}\vec{\sigma}^{asph}_{SM,x}+W^{sph}_{131,TM}\vec{\sigma}^{sph}_{TM,x}+W^{asph}_{131,TM}\vec{\sigma}^{asph}_{TM,x}, \\ \vec{A}_{131,y}&=W^{sph}_{131,SM}\vec{\sigma}^{sph}_{SM,y}+W^{asph}_{131,SM}\vec{\sigma}^{asph}_{SM,y}+W^{sph}_{131,TM}\vec{\sigma}^{sph}_{TM,y}+W^{asph}_{131,TM}\vec{\sigma}^{asph}_{TM,y}. \end{aligned} \tag{23}$$

Then all the lateral misalignments and angular misalignments can be determined through these sigma vectors. But figure errors have nothing to do with sigma

vectors. Some considerations should be taken to solve this problem.

5. Some considerations about the determination of figure errors

As is known, both alignment errors and figure errors have contributions to aberration fields. The primary problem is how to separate them. According to the NAT applied to freeform surfaces (*23*), the beam footprint at the surface is not the same for different field points. So, aberration contributions for different field points are varying. But the surface located at aperture stop (PM in TMA telescope) has the same footprint for different field points. In other words, wave-front aberrations contributed from figure errors of PM are independent of fields of view. Their contributions can be derived from the perturbation vectors, which are independent of fields of view (i.e. $\vec{B}^2_{222}$, $\vec{C}^3_{333}$).

If astigmatic figure errors on PM exist, the perturbation vector $\vec{B}^2_{222}$ in Equation (19) consists of two parts. It can be expressed as:

$$\vec{B}^2_{222} = {}_{Figure}\vec{B}^2_{222} + {}_{Align}\vec{B}^2_{222}, \tag{24}$$

where ${}_{Figure}\vec{B}^2_{222}$ denotes the contribution from figure errors, ${}_{Align}\vec{B}^2_{222}$ denotes the contribution from alignment errors. For TMA telescope, they can be expressed as:

$${}_{Figure}\vec{B}^2_{222} = 2(n - n')\begin{bmatrix} C_{5,PM} \\ C_{6,PM} \end{bmatrix}, \tag{25}$$

$$\begin{aligned} {}_{Align}\vec{B}^2_{222} = {} & W^{sph}_{222,SM}(\vec{\sigma}^{sph}_{SM})^2 + W^{asph}_{222,SM}(\vec{\sigma}^{asph}_{SM})^2 \\ & + W^{sph}_{222,TM}(\vec{\sigma}^{sph}_{TM})^2 + W^{asph}_{222,TM}(\vec{\sigma}^{asph}_{TM})^2. \end{aligned} \tag{26}$$

In Equation (25), $(n - n') = -2$, $C_{5,PM}$ and $C_{6,PM}$ denote the astigmatic figure errors on PM. In Equation (26), $W^{sph/asph}_{222,SM/TM}$ denotes the Seidel coefficients of SM and TM for TMA telescope. All the sigma vectors have been determined in the process of solving the alignment errors. So the astigmatic figure errors can be determined if $\vec{B}^2_{222}$ is solved in Equation (19).

For trefoil on PM, it can be determined according to the perturbation vector $\vec{C}^3_{333}$ in Equation (21). Its solving process is similar to the solving process of astigmatic figure errors on PM.

6. Simulations for the TMA telescopes

For the validation of the method presented in this paper, a TMA telescope is designed. As rendered in Figure 4, it is a 5 m F/16 telescope with a 0.2° × 0.1° field of view and a 0.15° field offset. This telescope is composed of PM, SM, TM, fine steering mirror (FSM) and image plane. Their optical parameters are listed in Table 1. And the corresponding Seidel aberration coefficients are listed in Table 2. Note that the aperture stop locates at PM and it is regarded as the reference surface.

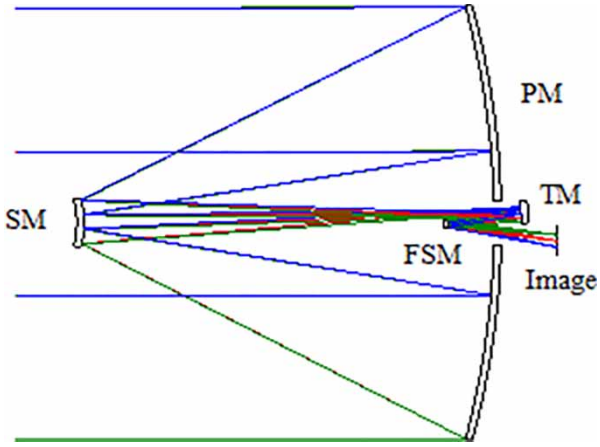

Figure 4. Layout of the TMA telescope.

Table 1. Optical prescription for the TMA telescope.

Surface	Type	Conic constant	Radius (mm)	Thickness (mm)	Decentre of the aperture
PM/stop	Conic	−0.996	−9999.588	−4500	
SM	Conic	−1.633	−1149.171	4800	
TM	Conic	−0.741	−1297.643	−900	123 mm
FSM			Infinity	1100	−26.8 mm
Image			Infinity		

Note: Note that the last column in Table 5 denotes the decentre of the aperture in *y* direction.

Table 2. Seidel coefficients of SM and TM for the TMA telescope.

	W^{sph}_{222}	W^{asph}_{222}	W^{sph}_{131}	W^{asph}_{131}
SM	−45.462	47.108	596.916	597.468
TM	77.699	−100.844	11.116	30.924

Theoretically, all the linear perturbation vectors ($\vec{A}_{klm}$) can be acquired by solving Equation (13), Equation (15), Equation (17), Equation (19) and Equation (21). Then sigma vectors can be determined by combining these linear perturbation vectors. In (*10*), two matrix equations similar to Equation (17) and Equation (19) are chosen to solve them. But the resulting values are biased from the designed. Therefore, the alignment method only based on aberration theory is undesirable. In this paper, we concentrate more on boresight error. On the premise that boresight errors are known, only two linear perturbation vectors are needed in the algorithm. The linear vectors associated with third-order aberrations are chosen here because they dominate the aberration fields. From Equation (17) and Equation (19), we can see that

four fields of view are enough to solve these matrix equations. At the same time, the axial misalignments can be calculated based on boresight errors.

In TMA telescope, SM and TM are likely to misalign. And PM figure may be damaged. To be in accordance with the realistic system, some small perturbations are introduced. The introduced alignment errors and figure errors are listed in Table 3. Among them, $XDE/YDE/ZDE$ denote the decentres of SM and TM, ADE/BDE denote the tilts of SM and TM, $C_{5,PM}/C_{6,PM}$ denote the astigmatic figure errors on PM, $C_{10,PM}/C_{11,PM}$ denote the trefoil figure errors on PM. After perturbation, the modulation transfer function (MTF) of the TMA telescope is depicted in Figure 5.

Through simulation, the computed alignment errors and figure errors are listed in Table 4. The MTF of the TMA telescope is depicted in Figure 6. From Table 4, we can see that the computed results are very close to the introduced. Specifically, the vertex decentres can be determined on the level of micron (even sub-micron), the tilts can be determined on the level of second (even sub-second), the figure errors can be determined on the level of 10^{-4} waves. From Figure 6, we can see that the system is diffraction limited. So a conclusion can be made that the perturbed TMA telescope has been recovered.

Table 3. The introduced alignment errors and figure errors.

XDE_{SM}/mm	YDE_{SM}/mm	ZDE_{SM}/mm	ADE_{SM}/°	BDE_{SM}/°
0.006	−0.004	0.008	0.0025	0.001
XDE_{SM}/mm	YDE_{SM}/mm	ZDE_{SM}/mm	ADE_{SM}/°	BDE_{SM}/°
0.005	−0.005	−0.007	−0.001	0.002
$C_{5,PM}$/waves	$C_{6,PM}$/waves	–	$C_{10,PM}$/waves	$C_{11,PM}$/waves
0.1	0.1	–	0.05	0.05

Table 4. The computed alignment errors and figure errors.

XDE_{SM}/mm	YDE_{SM}/mm	ZDE_{SM}/mm	ADE_{SM}/°	BDE_{SM}/°
0.006011	−0.004003	0.007912	0.002499	0.000999
XDE_{SM}/mm	YDE_{SM}/mm	ZDE_{SM}/mm	ADE_{SM}/°	BDE_{SM}/°
0.004887	−0.004930	−0.007053	−0.000997	0.002005
$C_{5,PM}$/waves	$C_{6,PM}$/waves	–	$C_{10,PM}$/waves	$C_{11,PM}$/waves
0.099737	0.099734	–	0.049897	0.049893

To further demonstrate the accuracy of the presented method in this paper, three cases of Monte Carlo simulations are conducted and analysed as listed in Table 5. There are 100 pairs of random perturbations following a standard uniform distribution for each case. Among them, Case 1 consists of relatively small values, Case 2 consists of relatively large values, Case 3 consists of the same values as Case 2 but with 1% measurement error.

An evaluation function should be set to evaluate these simulation results. Here we adopt the root mean square error (RMSE) between computed perturbations and introduced perturbations as the evaluation function. It can be expressed as:

$$RMSE = \sqrt{\frac{1}{N}\sum_{n=1}^{N}[X(n) - x(n)]^2}, \tag{27}$$

where $X(n)$ denotes the computed perturbation and $x(n)$ denotes the introduced perturbation. The resulting RMSE of every perturbation for different cases are listed in Table 6.

According to the simulations in Case 1 and Case 2, we can see that the calculated axial misalignments are the most accurate. The reason is that axial misalignments are mainly determined by boresight errors. They can be

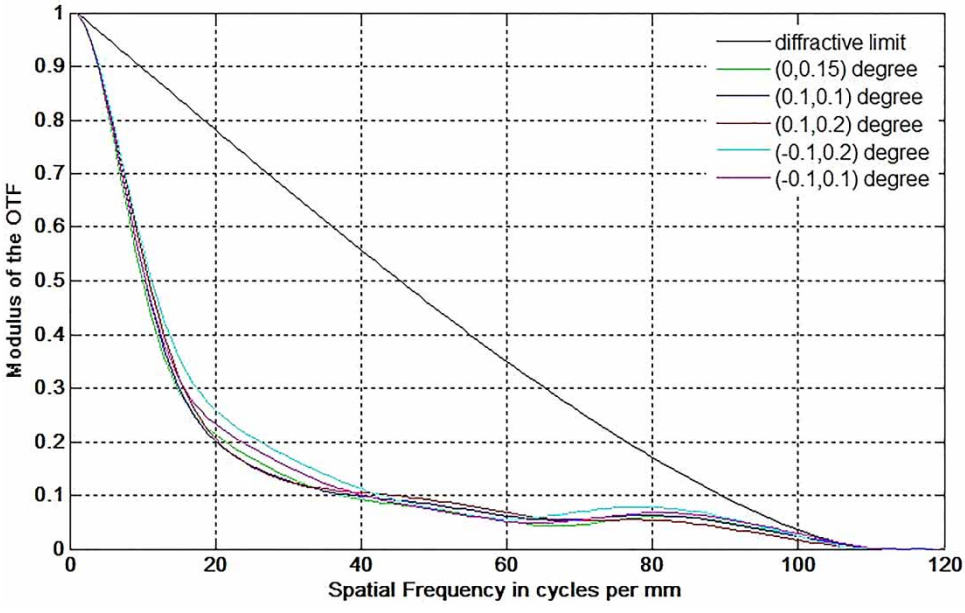

Figure 5. MTF of the TMA telescope before simulation.

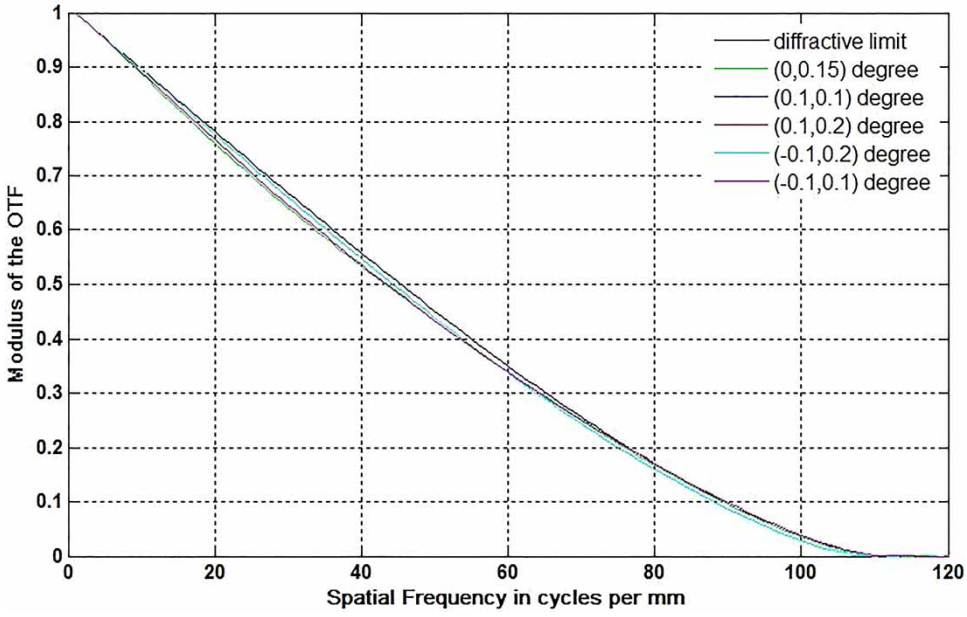

Figure 6. MTF of the TMA telescope after simulation.

Table 5. Ranges of perturbation used in Monte Carlo simulations.

	Axial misalignment (*ZDE*)	Lateral misalignment (*XDE*/*YDE*)	Angular misalignment (*ADE*/*BDE*)	Figure errors on PM ($C_5/C_6/C_{10}/C_{11}$)
Case 1	[−0.01,0.01]	[−0.01,0.01]	[−0.001,0.001]	[−0.01,0.01]
Case 2	[−0.1,0.1]	[−0.1,0.1]	[−0.01,0.01]	[−0.1,0.1]
Case 3	[−0.1,0.1]	[−0.1,0.1]	[−0.01,0.01]	[−0.1, 0.1]
	With 1% measurement error			

Table 6. The RMSE of every perturbation for different cases.

	Case 1	Case 2	Case 3
XDE_{SM}	2.29×10^{-6}	2.38×10^{-5}	7.22×10^{-4}
YDE_{SM}	9.12×10^{-7}	5.92×10^{-6}	1.45×10^{-3}
ZDE_{SM}	8.53×10^{-9}	1.22×10^{-8}	8.95×10^{-5}
ADE_{SM}	7.94×10^{-10}	5.15×10^{-9}	4.37×10^{-3}
BDE_{SM}	1.99×10^{-9}	2.07×10^{-8}	9.44×10^{-7}
XDE_{TM}	3.38×10^{-5}	4.24×10^{-4}	8.8×10^{-3}
YDE_{TM}	1.32×10^{-4}	1.63×10^{-4}	9.9×10^{-3}
ZDE_{TM}	2.14×10^{-7}	4.87×10^{-7}	1.41×10^{-3}
ADE_{TM}	1.02×10^{-7}	1.25×10^{-7}	7.91×10^{-6}
BDE_{TM}	2.60×10^{-8}	3.27×10^{-7}	4.79×10^{-6}
$C_{5,PM}$	1.54×10^{-5}	9.80×10^{-5}	2.29×10^{-4}
$C_{6,PM}$	9.42×10^{-6}	1.07×10^{-4}	2.48×10^{-4}
$C_{10,PM}$	6.37×10^{-5}	1.32×10^{-4}	7.13×10^{-4}
$C_{11,PM}$	5.73×10^{-5}	1.45×10^{-4}	9.96×10^{-4}

directly separated from the coupling effect. Furthermore, angular misalignments are relatively accurate compared with lateral misalignments and figure errors. The reason is that angular misalignments are mainly determined by sigma vectors contributed from spherical component, which are also determined by boresight errors. However, lateral misalignments and figure errors are mainly determined by field-dependent matrices. There exists coupling effect between them. They can only be determined by the singular value decomposition (SVD) of the field-dependent matrices.

Comparing Case 1 with Case 2, it is found that the computation accuracy declines as the perturbation parameters increase. This is because the alignment algorithm presented here is mainly based on the paraxial optics. It will become inapplicable with the increase of the perturbation parameters. But within the ranges in Case 2, the algorithm is still accurate and applicable.

In Case 3, 1% measurement errors are added. From the Monte Carlo simulation, we can see that the computation accuracy decreases compared to Case 2, especially the accuracy of axial misalignments and lateral misalignments. This is because aberration fields are mainly affected by angular misalignments and figure errors. Axial misalignments and lateral misalignments only have few contributions to the aberration fields. So it is difficult to precisely determine them in the presence of measurement errors. But the angular misalignments and the figure errors can be precisely determined. In this case, the perturbed TMA telescope can also be recovered with perfect performance.

7. Conclusion

In this paper, we present an algorithm about the active correction for the TMA telescope. Based on this algorithm, we can decouple the alignment errors of SM and TM. Meantime, we can decouple the figure errors of PM from the alignment errors of SM and TM.

Firstly, we analyse the advantages and disadvantages of the presented alignment algorithms. By contrast, the

algorithm based on NAT is regarded as the better one. Secondly, a vector called boresight error is introduced in this paper. This vector is independent of aberration coefficients. It plays an important role in decoupling. Thirdly, the field dependencies of third-order and fifth-order aberrations are expanded into matrix form here. Based on these matrices, it is easy to determine the perturbation vectors. Fourthly, we go into much detail about how to decouple the alignment errors and figure errors. Only by combining the boresight error with the field-dependent matrices, can the coupling effect be decoupled. In the end, a telescope system is designed to demonstrate the correctness of the method presented in this paper. By simulation, it is found that this algorithm owns high precision. Meantime, a Monte Carlo simulation is conducted to further demonstrate the accuracy of the algorithm. By analysis, we can see that the algorithm is applicable even in poor conditions.

However, several perturbation parameters are not discussed here. For example, the surface figure of SM and TM are likely to be damaged on orbit. Unlike PM, beam footprints on SM and TM are dependent with fields of view. They cannot be easily determined. Theories should be extended to solve these problems in the future.

Disclosure statement

No potential conflict of interest was reported by the authors.

Funding

This work was supported by the major innovation project of CIOMP [grant number Y3CX1SS14C].

References

(1) Tarenghi, M.; Wilson, R.N.. *Proc. SPIE* 1989, *1114*, 302–313.
(2) Chapman, H.N.; Sweeney, D.W. *Proc. SPIE* 1998, *3331*, 102–113.
(3) Liu, J.; Long, F.; Zhang, W. *Proc. SPIE* 2005, *5638*, 674–681.
(4) Kim, S.; Yang, H.S.; Lee, Y.W., Kim, S.-W., Eds. *Opt. Express* 2007, *15* (8), 5059–5068.
(5) Lee, H.; Dalton, G.B.; Tosh, I.A., Kim, S.-W., Eds. *Opt. Express* 2007, *15* (6), 3127–3139.
(6) Lee, H.; Dalton, G.B.; Tosh, I. A., Kim, S.-W., Eds. *Opt. Express* 2007, *15* (23), 15424–15437.
(7) Manuel, A.M. Field-Dependent Aberrations for Misaligned Reflective Optical Systems. Ph.D. Dissertation, University of Arizona, Tucson, Arizona, 2009.
(8) Schmid, T; Rolland, J.P.; Rakich, A.; Thompson, K.P. *Opt. Express* 2010, *18* (16), 17433–17447.
(9) Sebag, J.; Gressler, W.; Schmid, T.; Rolland, J.P.; Thompson, K.P. *Publ. Astron. Soc. Pac*. 2012, *124*, 380–390.
(10) Gu, Z.Y.; Yan, C.X.; Wang, Y. *Opt. Express* 2015, *23* (19), 25182–25201.
(11) Schmid, T.; Thompson, K.P.; Rolland, J.P. *Applied Opt*. 2010, *49* (16), D131.
(12) Hopkins, H.H. *The Wave Theory of Aberrations*; Clarendon: Oxford, 1950.
(13) Shack, R.V. Personal communication, Optical Sciences Center, University of Arizona, Tucson, AZ, 1987.
(14) Thompson, K.P.; Rolland, J.P. *Proc. SPIE* 2014, *9186*, 91860A.
(15) Thompson, K. *J. Opt. Soc. Am*. 2005, *22* (7), 1389–1401.
(16) Buchroeder, R.V. Tilted Component Optical Systems. Ph.D. Dissertation, University of Arizona, Tucson, AZ, 1976.
(17) Richards, K.; Rimmele, T.; Hegwer, S.L., Eds. *Proc. SPIE* 2010, *7736*, 773608.
(18) Upton, R.; Cho, M.; Rimmele, T. *Appl. Opt*. 2010, *49* (31), G105–G113.
(19) Gray, R.W.; Rolland, J.P. *J. Opt. Soc. Am*. 2015, *32*, 1836–1847.
(20) Thompson, K.P. *J. Opt. Soc. Am*. 2009, *26* (5), 1090–1100.
(21) Thompson, K.P. *J. Opt. Soc. Am*. 2010, *27* (6), 1490–1504.
(22) Thompson, K.P. *J. Opt. Soc. Am*. 2011, *28* (5), 821–836.
(23) Fuerschbach, K.; Rolland, J.P.; Thompson, K.P. *Opt. Express* 2012, *20* (18), 20139–20155.